RSC Advances

PAPER

Cite this: *RSC Adv.*, 2018, **8**, 24787

Sulfate radical-induced transformation of trimethoprim with $CuFe_2O_4$/MWCNTs as a heterogeneous catalyst of peroxymonosulfate: mechanisms and reaction pathways†

Jing Kong,[a] Ruobai Li,[a] Fengliang Wang,[a] Ping Chen,[b] Haijin Liu,[c] Guoguang Liu *[a] and Wenying Lv[a]

Received 14th May 2018
Accepted 16th June 2018

DOI: 10.1039/c8ra04103b

rsc.li/rsc-advances

Trimethoprim (TMP), a typical antibiotic pharmaceutical, has received extensive attention due to its potential biotoxicity. In this study, $CuFe_2O_4$, which was used to decorate MWCNTs *via* a sol–gel combustion synthesis method, was introduced to generate powerful radicals from peroxymonosulfate (PMS) for TMP degradation in an aqueous solution. The results showed that almost 90% of TMP was degraded within 24 min with the addition of 0.6 mM PMS and 0.2 g L^{-1} $CuFe_2O_4$/MWCNTs. The degradation rate was enhanced with the increase in initial PMS doses, catalyst loading and pH. A fairly low leaching of Cu and Fe was observed during the reaction, indicating the high potential recyclability and stability of $CuFe_2O_4$/MWCNTs. Electron paramagnetic resonance analysis confirmed that the $CuFe_2O_4$/MWCNT-PMS system had the capacity to generate ·OH and $SO_4^{\bullet-}$, whereas quenching experiments further confirmed that the catalytic reaction was dominated by $SO_4^{\bullet-}$. A total of 11 intermediate products of TMP was detected *via* mass spectrometry, and different transformation pathways were further proposed. Overall, this study showed a systematic evaluation regarding the degradation process of TMP by the $CuFe_2O_4$/MWCNT-PMS system.

1 Introduction

Currently, sulfate radical ($SO_4^{\bullet-}$)-based advanced oxidation processes (AOPs) have garnered increasing research interest as effective methods for the removal of various organic contaminants in aquatic environments.[1] The oxidizing potential of $SO_4^{\bullet-}$ is in the range of 2.5–3.1 V under different pH levels in solution, whereas it is only 1.9–2.7 V for the hydroxyl radical (·OH).[2] $SO_4^{\bullet-}$ may be generated by the activation of peroxymonosulfate (PMS) with transition metals (*e.g.*, Fe^{2+}, Cu^{2+}, Co^{2+}),[3] metal oxides,[4] and heating,[5] which is very promising for large-scale wastewater treatment. Among these methods, the transition metal activation of PMS has two advantages, *i.e.*, it is easy to operate and energy saving. However, the homogeneous system results in the discharge of dissolved heavy metals into the environment. The toxicity and the potential carcinogenicity of leaching cations limit their practical environmental protection applications. Therefore, it is necessary to prepare a highly stable and recyclable catalyst to produce $SO_4^{\bullet-}$.

$CuFe_2O_4$ exhibits effective catalytic activity for PMS-generated $SO_4^{\bullet-}$.[6] In addition to the ease of recycling, another advantage of $CuFe_2O_4$ is its magnetic nature, which makes its separation from aqueous systems quite straightforward. Nevertheless, the unique magnetic properties of $CuFe_2O_4$ lead to particulate aggregation, which limits the conductivity and the population of active sites.[7] The loading of $CuFe_2O_4$ onto carbonaceous materials not only limits the aggregation of $CuFe_2O_4$ nanoparticles, but also provides additional active sites and facilitates electron transfer within the system.[8,9] Compared to other carbon materials (*e.g.*, activated carbon and graphite), multi-walled carbon nanotubes (MWCNTs) have unique properties such as chemical stability and extreme strength.[10,11] In a previous study, Zhang *et al.* used a multi-walled carbon nanotube-loaded $CuFe_2O_4$ (CNTs/$CuFe_2O_4$)-PMS system for the degradation of 2-phenylbenzimidazole-5-sulfonic acid (PBSA), and they found that this composite exhibited good catalytic activity and stability.[12]

Pharmaceuticals and personal care products (PPCPs) in ambient aquatic environments have been a growing concern due to their ubiquitous occurrence and potential negative impacts on ecosystems and human health.[13] Pharmaceuticals and their bioactive metabolites are being continuously introduced into natural aquatic systems through the incomplete

[a]School of Environmental Science and Engineering, Guangdong University of Technology, Guangzhou 510006, China. E-mail: liugg615@163.com; Fax: +86-20-3932-2548; Tel: +86-13533635690

[b]School of Environment, Tsinghua University, Beijing 100084, China

[c]School of Environment, Henan Normal University, Henan Key Laboratory for Environmental Pollution Control, Xinxiang 453007, China

† Electronic supplementary information (ESI) available. See DOI: 10.1039/c8ra04103b

decomposition of urban sewage and excretions from the human body.[14,15] Trimethoprim (TMP) as a broad-spectrum antibiotic is employed to treat various bacterial infections including otitis media, gastrointestinal, respiratory, and urinary infections.[16,17] The reported concentrations of TMP are 0.1–5 μg L^{-1}, 2.2–10.9 ng L^{-1}, and 0–19.8 ng L^{-1} in wastewater treatment plant effluents, surface water, and finished drinking water, respectively.[18] Therefore, technologies that can effectively remove TMP have been attracting increasing attention. Until now, various methods have been performed for the removal of TMP from water. Zhang *et al.* demonstrated that the UV/PDS system can efficiently degrade TMP.[19] Wang *et al.* found that the homogenous Fe^{2+}/PS process showed an efficient TMP removal in an aqueous solution.[20] However, the degradation of TMP using a $CuFe_2O_4$/MWCNT-PMS heterogeneous system has not been attempted yet.

In this study, a $CuFe_2O_4$/MWCNT composite was synthesized through a facile method and applied as a heterogeneous activator towards PMS. The catalytic degradation mechanism of TMP as well as the reusability of the $CuFe_2O_4$/MWCNT composite was systematically investigated. Furthermore, detailed mechanisms and transformation pathways for TMP degradation by the $CuFe_2O_4$/MWCNT-PMS system were proposed based on the intermediate product identification by liquid chromatography–tandem mass spectrometry (HPLC/MS/MS), reactive oxygen species detection, and XPS.

2 Experimental section

2.1 Preparation and characterization

The $CuFe_2O_4$/MWCNT composite was synthesized according to a previously reported method with slight improvement. Detailed information regarding the preparation and characterization methods of the catalyst is provided in Text S1.†

2.2 Experimental procedures

Degradation experiments were performed in a 250 mL bath reactor at 27 °C, and the initial pH was set at 7.0. Next, 0.02 mM TMP and 0.2 g L^{-1} of $CuFe_2O_4$/MWCNTs were added to a 100 mL reaction resolution, where the reaction was initiated by the addition of 0.6 mM PMS. Samples (5 mL) of the solution were extracted at 0, 1, 2, 4, 8, 16, and 24 min time intervals, quenched by 0.6 mM $Na_2S_2O_3 \cdot 5H_2O$, and immediately filtered with a 0.45 μm filter into a 1 mL brown vial for HPLC analysis. Other influencing elements for the catalytic degradation of TMP were evaluated in the same way.

2.3 Analysis of TMP degradation

The concentration of TMP was analyzed *via* a HPLC-UV detector at a wavelength of 239 nm. The column that was used in the experiment was a Chromolith Performance XDB-C18 column (150 × 4.6 mm, 5-micron, Agilent, USA). The oven temperature was set at 35 °C, and the injection volume was 20 μL. The mobile phase was a mixture of acetonitrile and 0.2% methanoic acid in water (85 : 15, v/v) with a flow rate of 0.2 mL min^{-1} under isocratic conditions. The total organic carbon (TOC) was measured by a TOC-V_{CPH} analyzer (Japan) to identify the mineralization of the organic contaminants. The analysis of the products is shown in Text S1 of the ESI.†

3 Results and discussion

3.1 Characterization of catalysts

The morphologies of $CuFe_2O_4$/MWCNTs were revealed by TEM observation (Fig. 1a). Furthermore, carbon was detected using the elemental mapping results (Fig. 1b–e) following the synthesis, which indicated the successful loading of $CuFe_2O_4$ MNPs onto MWCNTs. The N_2 adsorption–desorption isotherms and the pore size distribution are shown in Fig. 1h, indicating the presence of interparticle meso-porosity in this material.[21] In addition, the specific surface areas (SSAs) of $CuFe_2O_4$/MWCNTs (84.3 m^2 g^{-1}) were far higher than that of bulk $CuFe_2O_4$ (29.7 m^2 g^{-1}). The XRD patterns in Fig. 1f show that both MWCNTs and $CuFe_2O_4$/MWCNTs displayed a characteristic peak at $2\theta = 26°$, which revealed that their carbon skeletons were maintained during the synthesis.[22] The diffraction peaks for $CuFe_2O_4$/MWCNTs were similar to the standard diffraction data for $CuFe_2O_4$ (JCPDS 34-0425).[23] The diffraction peaks of $CuFe_2O_4$/MWCNTs were narrower than that of bare $CuFe_2O_4$, which indicated particle aggregation during annealing.[23] As expected in FT-IR spectra (Fig. 1g), the absorption band in the 1700–1600 cm^{-1} region was assigned to the stretching vibration of C=O in both pristine MWCNTs and $CuFe_2O_4$/MWCNTs;[24] this indicated that the carboxylic groups remained after being calcined, which is critical for the catalyst for preserving the hydrophilicity and high dispersibility. Magnetic hysteresis (M-H) curves for both pristine and used $CuFe_2O_4$/MWCNTs (Fig. 1i) demonstrated that the used catalyst still possessed a high level of magnetism.

The above-mentioned results illustrated the structure, morphology and physical characteristics of the $CuFe_2O_4$/MWCNT composites, which indicated that MWCNTs were successfully coupled with the $CuFe_2O_4$ surface. Furthermore, due to the excellent magnetic properties of the catalysts, we could easily separate them under a magnetic field, which is very beneficial for recycling.

3.2 Degradation of TMP by the $CuFe_2O_4$/MWCNT-PMS system

3.2.1 High catalytic activity of $CuFe_2O_4$/MWCNTs. To comprehensively evaluate the catalytic degradation performance of $CuFe_2O_4$/MWCNTs, Fig. 2a shows the TMP degradation *via* a series of experiments. The addition of 0.6 mM PMS in the absence of any catalyst brought about 23% of TMP removal in 24 min, which indicated the excellent oxidizing capacity of PMS. Meanwhile, the simultaneous use of 0.2 g L^{-1} $CuFe_2O_4$/WMCNTs and 0.6 mM PMS resulted in a TMP removal of 89% in 24 min, which was higher than that observed with 0.2 g L^{-1} $CuFe_2O_4$ (69%) and MWCNTs (52%). These results indicated that the $CuFe_2O_4$/WMCNTs composite possessed excellent degradation performance toward TMP in the presence of PMS. Moreover, the adsorptions of TMP by $CuFe_2O_4$/WMCNTs, $CuFe_2O_4$ and MWCNTs were measured to be 2%, 3%, and 31%, respectively.

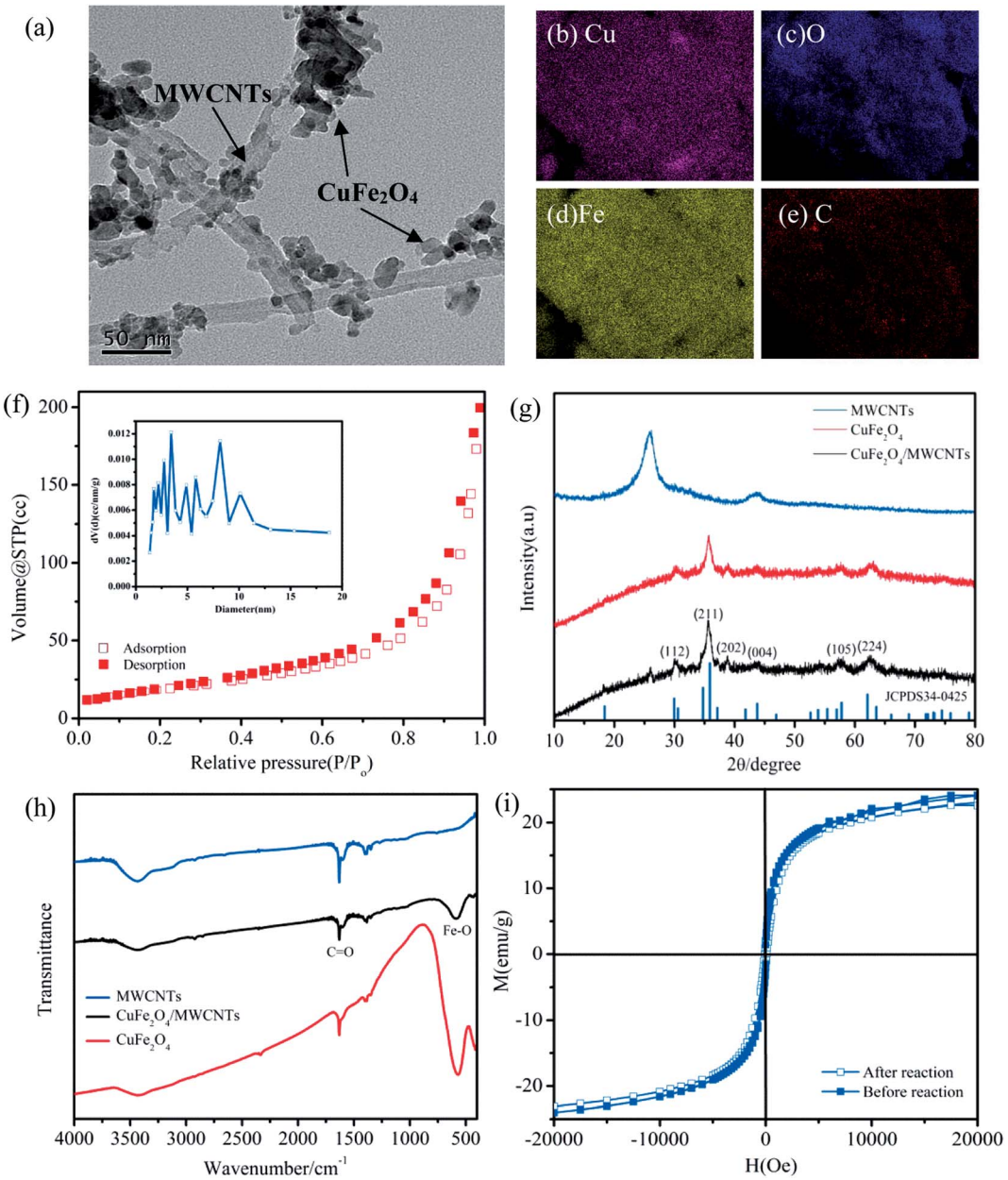

Fig. 1 (a) The TEM image and (b–e) elemental mapping of $CuFe_2O_4$/MWCNTs; (f) N_2 adsorption–desorption isotherms and the corresponding pore size distribution (inset) of $CuFe_2O_4$/MWCNTs; (g) XRD patterns of the three samples; (h) FT-IR spectra of the three samples; (i) M-H loops of $CuFe_2O_4$/MWCNTs before and after the reaction.

The adsorption effect of $CuFe_2O_4$/WMCNTs was less than that of MWCNTs. The lower absorption rate of the $CuFe_2O_4$/MWCNT composites might have been due to the fact that $CuFe_2O_4$ nanoparticles occupied the adsorption sites of MWCNTs.

3.2.2 Effects of initial PMS concentration and catalyst doses. The TMP degradation was enhanced with the increase in the initial PMS concentration within the scale of the experiment.. As shown in Fig. 2b, the degradation efficiency of TMP was 80% at 0.2 mM PMS after 24 min, and it continued to increase to 89% at 0.6 mM PMS. The degradation efficiency decreased to 65% by increasing the initial concentration of PMS to 1 mM. It could be observed that the active sites on the surfaces of $CuFe_2O_4$/WMCNTs were not totally occupied by PMS at a concentration of 0.6 mM. The radical scavenging ability of PMS and the quantities of $SO_4^{\bullet -}$ ions quenched by their self-coupling reactions also increased with higher initial PMS concentrations. Similar conclusions were also obtained by Zhang *et al.*[12] when they studied the degradation of organic pollutants by PMS.

The degradation of TMP under different catalyst doses (0.1, 0.2, and 0.3 g L^{-1}) was investigated, and the results are shown in Fig. 2c. According to Fig. 2c, the increasing catalyst loading could promote the degradation of TMP. At the catalyst doses were varied from 0.1 g L^{-1} to 0.3 g L^{-1}, the degradation

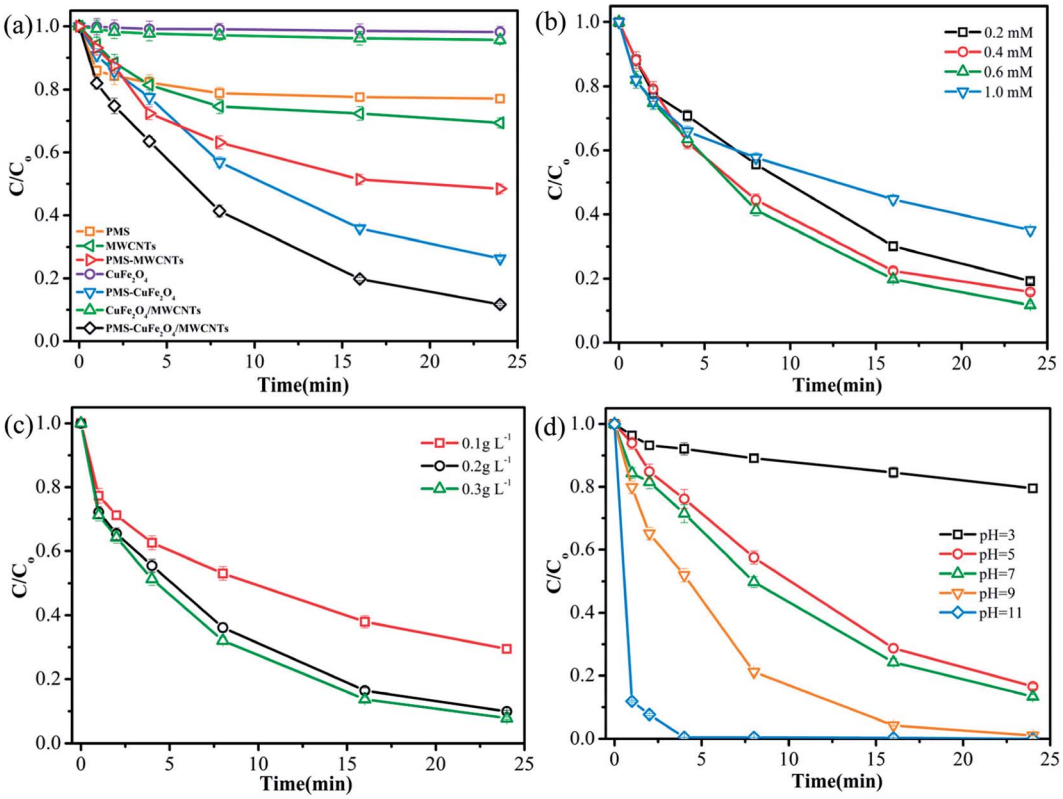

Fig. 2 (a) TMP removal efficiencies by various reactions; effects of (b) initial PMS concentration; (c) catalyst dose and (d) initial pH on TMP degradation. Reaction conditions: initial TMP concentration, 0.02 mM; PMS, 0.6 mM; catalyst dose, 0.2 g L^{-1}; pH = 7.0; temperature, 27 °C.

efficiency of TMP improved by about 20%. In a previous study, the decontamination rate attained a maximum and then decreased with the continuously increasing $CuFe_2O_4$ catalyst load, which suggested that the detrimental effects of high doses of the catalyst were suppressed by its stimulation effects.[6]

3.2.3 Effects of initial solution pH. A complex role was played by pH in the catalytic TMP degradation process. As presented in Fig. 2d, the efficiency of TMP degradation was found to be significantly enhanced as the initial pH value was raised from 3 to 11. A previous study noted that the addition of acid PMS can lead to a significant decrease in the solution pH.[25] In addition, pH variations during the reaction were roughly monitored (Fig. S3†). The initial pH of 11 decreased over time and finally remained above pH 7.5. Similar results were obtained by Guan *et al.*[6] Furthermore, the catalyst had a net positive (negative) charge at a pH that was lower (higher) than pH_{PZC}, whereas the net particle charge was zero at a pH around pH_{PZC} (pH at the point of zero charge). The pH_{PZC} values of $CuFe_2O_4$ and $CuFe_2O_4$/MWCNTs were measured to be 8.6 and 7.3, respectively. As depicted in Fig. S2,† the existing forms of PMS and TMP were primarily contingent on the pH and the pK_a of the solution. The pK_{a1} and pK_{a2} values of TMP were 3.2 and 7.1, respectively, whereas the pK_a value for PMS was 9.4.[26] Thus, in the pH range from 0 to 7.5, PMS mostly existed in the form of HSO_5^- (transformed to $SO_4^{\bullet-}$), whereas TMP mainly existed as H_2TMP^+ and $HTMP^0$. It is worthy of note that the rapid increase in the degradation rate with the increase in initial pH from 9 to 11 was somewhat unexpected. The main reasons are as follows: First, an increase in liberated OH^- ions in the solution might also accelerate the decomposition of PMS to form ·OH, which react with organics in a non-selective manner.[27] Second, TMP mainly exists in the molecular form in this pH range, and the highly electronegative N atom of the amino group can be easily attacked by ·OH. On the other hand, the self-decomposition of PMS rapidly occurs under strongly alkaline conditions, producing highly oxidizing species. Moreover, the low degradation rate at pH 3 and pH 5 is likely due to acid-catalyzed PMS decomposition, which depletes PMS without the production of radicals.[28]

3.3 Recyclability of $CuFe_2O_4$/MWCNTs and cation leaching

The recyclability of the $CuFe_2O_4$/MWCNT catalyst is crucial in the practical applications. The degradation experiments were repeated for four cycles to evaluate the catalytic stability of $CuFe_2O_4$/MWCNTs. After being used, the $CuFe_2O_4$/MWCNT catalyst was magnetically collected and dried. As shown in Fig. 3, the removal efficiency remained at around 82% after four cycles, suggesting the high stability of $CuFe_2O_4$/MWCNTs in the PMS oxidation system. Moreover, the leaching of Cu as well as Fe was measured during the time course of TMP degradation with the addition of 0.2 g L^{-1} catalysts. Under reaction conditions, the atomic absorption spectroscopy (AAS) analysis indicated that the leaching of Cu was about 0.13 mg L^{-1} over 60 min, which

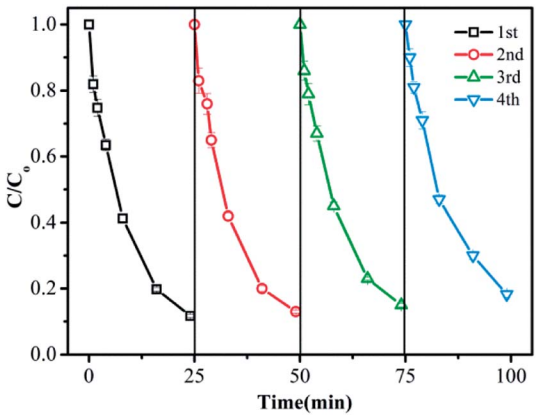

Fig. 3 Recyclability of the catalyst for TMP removal in four runs. Reaction conditions: initial TMP and PMS concentrations were 0.02 mM and 0.6 mM, respectively. Catalyst dose, 0.2 g L^{-1}; pH = 7.0; temperature, 27 °C.

accounted for 0.065% of the total Cu content in the catalyst, whereas the leaching of Fe was less than 0.04 mg L^{-1}.

3.4 Activation mechanism of the catalyst

PMS has the capacity to generate three primary types of reactive radicals ($SO_4^{\cdot-}$, $SO_5^{\cdot-}$ and ·OH) through metal-ion activation.[29] The species of radicals generated from the oxidation of TMP were probed by the DMPO spin-trapping EPR technique. As shown in the EPR spectrum (Fig. 4a), no distinctive radical was produced by DMPO; the EPR signals represented the presence of DMPO-OH and DMPO-$SO_4^{\cdot-}$ adducts.[30,31] Thus, ·OH and $SO_4^{\cdot-}$ were shown to be involved in the catalytic degradation process.[32] To further identify the types of major reactive radical species generated in the degradation system, ethanol (EtOH) and *tert*-butyl alcohol (TBA) were added into the reaction solution as radical quenching agents. EtOH (containing α-hydrogen) reacted with ·OH and $SO_4^{\cdot-}$ at high and comparable rates, where the rate constants for the reactions with ·OH and $SO_4^{\cdot-}$ were 1.2–2.8 × 10^9 mol L^{-1} s^{-1} and 1.6–7.7 × 10^7 mol L^{-1} s^{-1}, respectively. However, the rate constant of TBA (without α-hydrogen) with ·OH was 1000 times higher compared to that with $SO_4^{\cdot-}$.[22] Therefore, EtOH was employed to quench both ·OH and $SO_4^{\cdot-}$, and TBA was applied to selectively quench ·OH. As depicted in Fig. 4b, when no quenching agents were added, about 90% of TMP degraded in 24 min. In contrast, the addition of 0.3 mol L^{-1} of EtOH and TBA to the reaction significantly decreased the degradation efficiencies to 21% and 58%, respectively. The addition of more EtOH and TBA further decreased the TMP removal and when their concentrations were fixed at 0.6 mol L^{-1}, the removal rates of TMP were only 15% and 45%, respectively. The enhanced decrease in the TMP removal by EtOH rather than that by TBA suggested that the primary radical species generated during the activation of PMS was $SO_4^{\cdot-}$.

To better understand the roles of Fe and Cu in the activation of PMS, XPS spectra were obtained prior to and following the catalytic reaction (Fig. 5). The results showed that the valence of Fe^{3+} on the surface of $CuFe_2O_4$/MWCNTs did not change after the reaction. Ren *et al.* reported a similar conclusion, which stated that only the metals in the A site had a valence change on the surface of MFe_2O_4.[33] Fig. 5c shows a peak at 934.001 eV before the catalytic reaction, which was assigned to Cu $2p_{3/2}$ of Cu^{2+}; this value slightly shifted to a lower binding energy value (933.9 eV) following the catalytic reaction, which indicated that the valence of Cu on the surface of the catalyst after the reaction was a combination of the valences of Cu^{2+} and Cu^{+}. Based on the characteristic peaks, the relative contributions of Cu^{2+} and Cu^{3+} accounted for about 40% and 26%, respectively.[22] Cu species were mainly present as Cu^{2+} before the reaction, and they were transformed to Cu^{3+} and several Cu^{+} ions following the catalytic reaction, which might have been due to the coexisting oxidation and reduction conditions in the solution.

The mechanism for the activation of PMS by $CuFe_2O_4$/MWCNTs was proposed as follows (eqn (1)–(7)):

$$\equiv Cu^{2+} + HSO_5^- \rightarrow \equiv Cu^{3+} + SO_4^{\cdot-} + OH^- \quad (1)$$

$$\equiv Cu^{2+} + HSO_5^- \rightarrow \equiv Cu^{+} + SO_4^{\cdot-} + H^+ \quad (2)$$

$$\equiv Cu^{+} + HSO_5^- \rightarrow \equiv Cu^{2+} + SO_4^{\cdot-} + OH^- \quad (3)$$

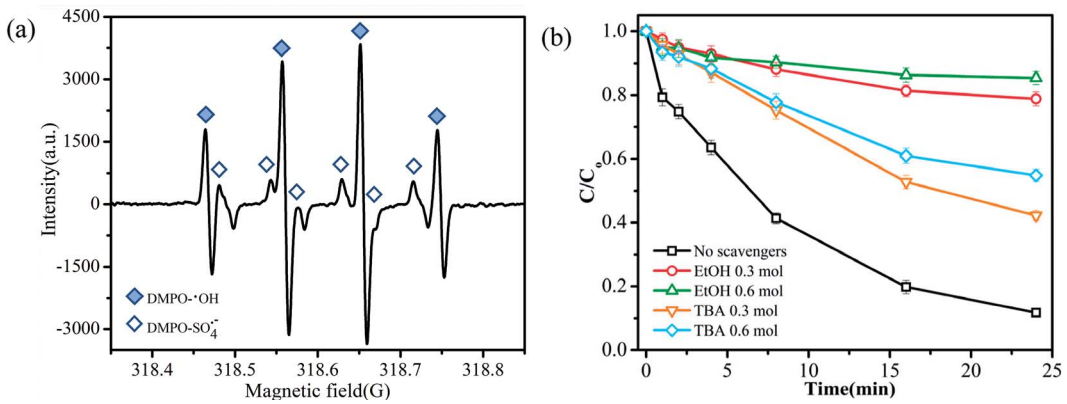

Fig. 4 (a) EPR spectrum of the $CuFe_2O_4$/MWCNT-PMS system (C_{DMPO} = 50 mM); (b) effects of quenchers on TMP degradation. Reaction conditions: initial TMP and PMS concentrations were 0.02 mM and 0.6 mM, respectively. Catalyst dose 0.2 g L^{-1}; pH = 7.0, temperature was 27 °C.

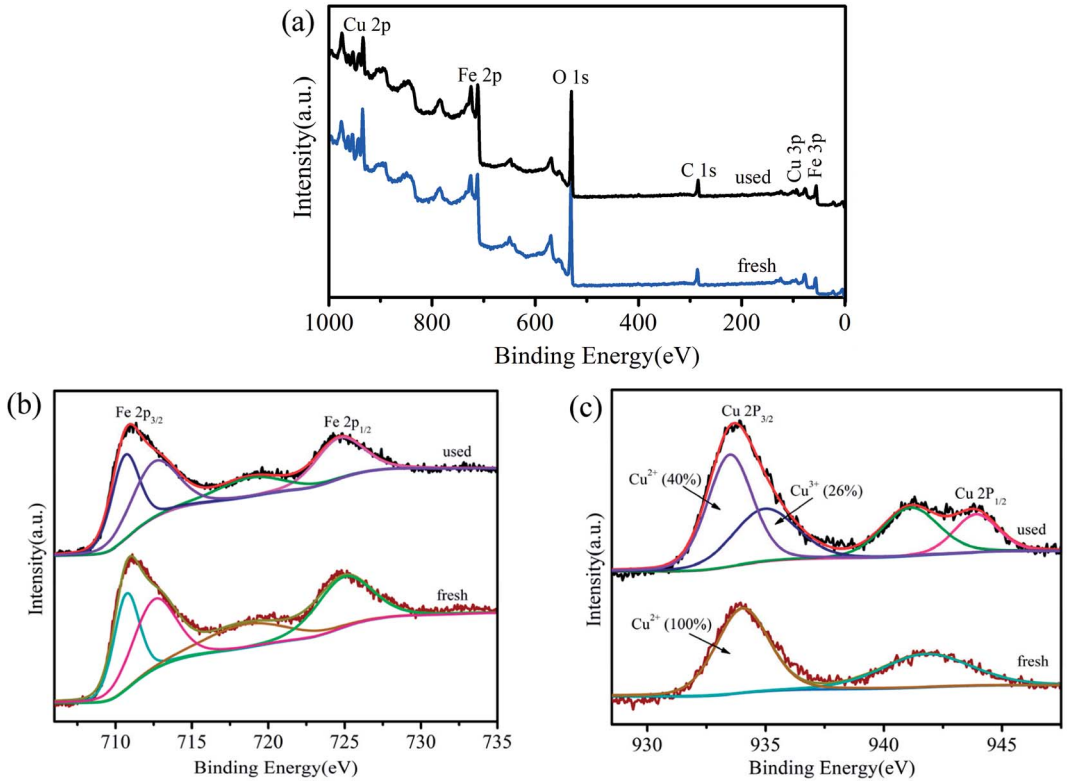

Fig. 5 (a) Wide survey XPS spectrum; (b) Fe 2p and (c) Cu 2p XPS envelopes of used and fresh catalysts.

$$\equiv Cu^{3+} + HSO_5^- \rightarrow \equiv Cu^{2+} + SO_5^{\cdot -} + H^+ \quad (4)$$

$$SO_4^{\cdot -} + TMP \rightarrow \text{degraded products} \rightarrow H_2O + CO_2 \quad (5)$$

$$SO_4^{\cdot -} + H_2O \rightarrow SO_4^{2-} + H^+ + \cdot OH \quad (6)$$

$$\cdot OH + TMP \rightarrow \text{degraded products} \rightarrow H_2O + CO_2 \quad (7)$$

Interestingly, the oxidation of HSO_5^- by Cu^{2+} was thermodynamically unfavorable (eqn (2)) (Cu^{2+}/Cu^+ (0.17 V) and SO_5^{2-}/HSO_5^- (1.1 V) or $SO_5^{\cdot -}/SO_5^{2-}$ (0.81 V));[34] however, the reactions were still possible as $SO_5^{\cdot -}$ was at a low concentration, which rendered the actual reduction potential of SO_5^{2-}/HSO_5^- or $SO_5^{\cdot -}/SO_5^{2-}$ to a relatively low value in the catalyst system. However, due to the weak oxidizing ability of $SO_5^{\cdot -}$ ($E(SO_5^{\cdot -}/SO_4^{2-}) = 1.1$ V), it was considered that it did not contribute to TMP degradation.[35] Cu^+ could be oxidized by HSO_5^- (eqn (3)), which was an additional pathway for the generation of $SO_4^{\cdot -}$, and it also returned the metal centers to their initial oxidation states for the next catalytic cycle.

On the basis of the experimental results mentioned above, the potential activation mechanism was concluded. When PMS was added, $SO_4^{\cdot -}$ and $\cdot OH$ were generated from PMS, which was activated by the unveiled active sites of Cu^{2+}.[36] During this process, PMS could also be activated by MWCNTs to generate additional reactive species through non-radical reactions.[37,38] In addition, owing to the highly electronic conductive trait of MWCNTs, they facilitated the electron transfer between metal ions.[39] To balance the charge on the $CuFe_2O_4$/MWCNT surface, Cu^{2+} not only provided electrons, but also accepted the electrons from the system, which indicated the involvement of Cu^{2+}–Cu^{3+}–Cu^{2+} and Cu^{2+}–Cu^+–Cu^{2+} redox processes during the reaction.[33] Finally, TMP was adsorbed onto the surface of the $CuFe_2O_4$/MWCNT catalyst, which was attacked by $SO_4^{\cdot -}$ and $\cdot OH$, leading to decomposition and mineralization.

3.5 Degradation transformation products and pathways

TMP was degraded into a variety of transformation products, as identified by the HPLC/MS/MS technique. A positive full scan mass spectrum of SPE enrichment revealed the by-products of TMP that were detected in the $CuFe_2O_4$/MWCNT-PMS system. For TMP degradation, the potential transformation pathways are shown in Fig. 6. As seen, hydroxylation, the cleavage of methylene groups, and demethylation were proposed to be existing in this system. Among them, hydroxylation was the most prominent pathway. Moreover, the free radicals reacted relatively easily with $–CH_2–$ group-generated carbon centers; the cleavage of the methylene bridge was another major pathway. Furthermore, demethylation was often accompanied with hydroxylation. These proposed TMP pathways likely included different reaction mechanisms. On the basis of previous results, we inferred that TMP was primarily destroyed by $SO_4^{\cdot -}$ and $\cdot OH$. The $SO_4^{\cdot -}$ ions preferentially reacted through an electron transfer process, whereas $\cdot OH$ reacted *via* hydrogen abstraction or addition reactions.[40] Detailed MS^2 spectra and the proposed structures of TMP and each by-product are provided in the ESI.†

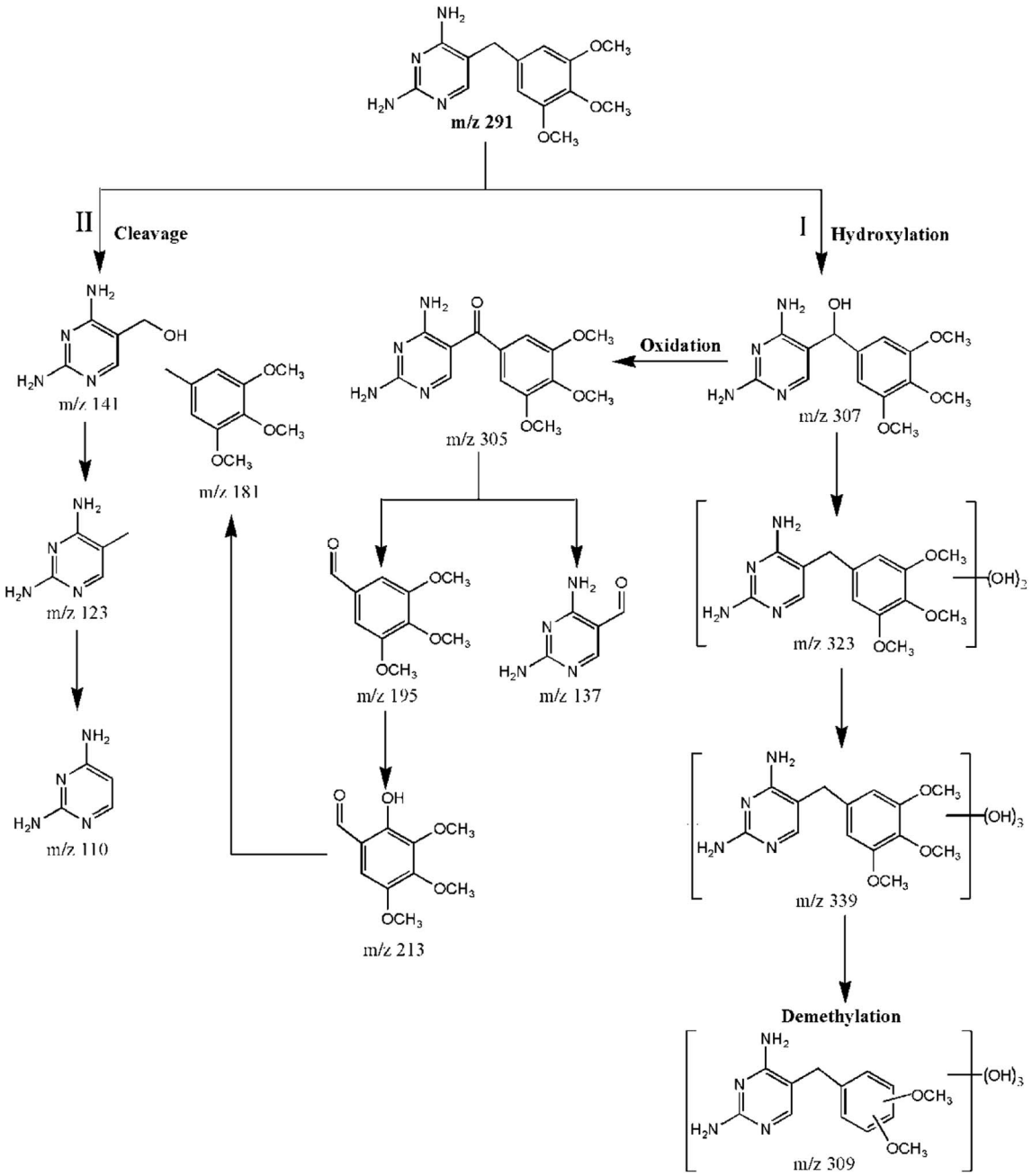

Fig. 6 Proposed transformation pathways for TMP degradation.

Pathway I is hydroxylation by which hydroxyl groups can be attached to either the ring of the TMP molecule or to the methylene bridge. The products at *m*/*z* 307 (P4) and 305 (P5) were identified as α-hydroxytrimethoprim and α-keto-trimethoprim, respectively. The fragment ions at *m*/*z* 289 and *m*/*z* 274 of the P4 (Fig. S5f†) implied that a hydroxyl group was added to the C-7 atom; otherwise, the hydroxyl groups on either aromatic ring would lack a hydrogen on the β-atom, which is essential for the formation of a double bond.[41] P4 and P5 were likely generated by the electron transfer mechanism and the attack by $SO_4^{\cdot-}$.[42] Furthermore, P4 reacted with $SO_4^{\cdot-}$ and was oxidized to P5. These two compounds were previously identified as transformation products of TMP using the UV-PS system,[42] Fe^0-PS system[43] and permanganate treatment.[44] The additional value of 32 amu relative to TMP (*m*/*z* 291) suggested that the products at *m*/*z* 323 (P2) were dihydroxylated isomers on the basis of TMP;[43] thus, they possessed several positional isomers. Fig. S5c† and d shows only the MS^2 spectra of two isomers, and *m*/*z* 339 (P1) possessed a molecular weight that was 16 amu higher than that of P2, which suggested a transformation pathway of hydroxylation. Compared to P1, P3 (*m*/*z* 309) lost one methoxy group. P2, P1, and P3 were the products that were generated by the direct addition of ·OH.

Pathway II included the cleavage of the C–C bond between the two rings in TMP, which was due to a direct attack by $SO_4^{\cdot-}$ or ·OH at the methylene bridge. The cleavage of the methylene

group generated m/z 141 (P7) and m/z 181 (P9), and a similar reaction also occurred for P5. The fragmentation pathway of P5 was consistent with those proposed by Ji *et al.*[45] For P7, m/z 123 (P10) could be explained by the loss of water; this ion could be stabilized by mesomeric resonance. The value of m/z 123 or 110 (P11) corresponded to the characteristic fragments of protonated TMP containing pyrimidine groups (Table S1†).[10] In addition, P9 was proposed to be a pseudo-molecular ion of the trimethoxytoluene moiety.

During the TMP oxidation process, TOC removal was measured to reflect the mineralization of TMP. After 2 hours, TMP was completely decomposed, but the TOC removal was approximately 35% (Fig. S4†). These results indicated that TOC reduction proceeded much more slowly than the degradation of TMP. Most of the by-products generated during the degradation of TMP maintained the two-ring TMP structure, which could account for this phenomenon.

4 Conclusions

Magnetic porous $CuFe_2O_4$/MWCNTs were synthesized by a sol–gel combustion method, and they were fully characterized. The synergistic effects of $CuFe_2O_4$ and MWCNTs facilitated the activation of PMS to decompose TMP, showing the notable catalytic performance of $CuFe_2O_4$/MWCNTs. In addition, $CuFe_2O_4$/MWCNTs exhibited good stability with low levels of metal cation leaching. An investigation of the reaction parameters revealed that the PMS dosage, catalyst loading, and initial pH had influences on the degradation efficiency of TMP to a large extent. The results of EPR and quenching experiments proved that both $\cdot OH$ and $SO_4^{\cdot -}$ participated in the degradation of TMP, whereas $SO_4^{\cdot -}$ was the primary radical species. The major transformation pathways were proposed to be hydroxylation, cleavage of methylene group and demethylation. This is the first time that the $CuFe_2O_4$/MWCNT-PMS system was evaluated by investigating the degradation mechanisms of pharmaceuticals, which provided more insights into a new catalyst for advance oxidation processes. Overall, this systematic investigation presented a promising heterogeneous catalyst for practical applications in the treatment of pharmaceutical wastewater and drinking water.

Conflicts of interest

There are no conflicts to declare.

Acknowledgements

This work was supported by the National Natural Science Foundation of China [No. 21377031 and 21677040]; and the Innovative Team Program of High Education of Guangdong Province [2015KCXTD007].

References

1 Y. Yao, H. Chen, J. Qin, G. Wu, C. Lian, J. Zhang and S. Wang, *Water Res.*, 2016, **101**, 281–291.
2 P. Neta, R. E. Huie and A. B. Ross, *J. Phys. Chem. Ref. Data*, 1988, **17**, 1027–1284.
3 G. P. Anipsitakis and D. D. Dionysiou, *Environ. Sci. Technol.*, 2004, **38**, 3705–3712.
4 G. D. Fang, D. D. Dionysiou, S. R. Al-Abed and D. M. Zhou, *Appl. Catal., B*, 2013, **129**, 325–332.
5 M. Nie, Y. Yang, Z. Zhang, C. Yan, X. Wang, H. Li and W. Dong, *Chem. Eng. J.*, 2014, **246**, 373–382.
6 Y. H. Guan, J. Ma, Y. M. Ren, Y. L. Liu, J. Y. Xiao, L. Q. Lin and C. Zhang, *Water Res.*, 2013, **47**, 5431.
7 Y. Q. Wang, R. M. Cheng, Z. Wen and L. J. Zhao, *Eur. J. Inorg. Chem.*, 2011, **2011**, 2942–2947.
8 X. M. Chen, Z. J. Lin, T. T. Jia, Z. M. Cai, X. L. Huang, Y. Q. Jiang, X. Chen and G. N. Chen, *Anal. Chim. Acta*, 2009, **650**, 54–58.
9 Y. Yao, Y. Cai, F. Lu, F. Wei, X. Wang and S. Wang, *J. Hazard. Mater.*, 2014, **270**, 61–70.
10 X. Hu, B. Liu, Y. Deng, H. Chen, S. Luo, C. Sun, P. Yang and S. Yang, *Appl. Catal., B*, 2011, **107**, 274–283.
11 Y. Yao, H. Chen, C. Lian, F. Wei, D. Zhang, G. Wu, B. Chen and S. Wang, *J. Hazard. Mater.*, 2016, **314**, 129–139.
12 X. Zhang, M. Feng, L. Wang, R. Qu and Z. Wang, *Chem. Eng. J.*, 2017, **307**, 95–104.
13 L. P. Padhye, H. Yao, F. T. Kung'U and C. H. Huang, *Water Res.*, 2014, **51**, 266.
14 C. Sirtori, A. Agüera, W. Gernjak and S. Malato, *Water Res.*, 2010, **44**, 2735–2744.
15 F. Wang, P. Chen, Y. Feng, Z. Xie, Y. Liu, Y. Su, Q. Zhang, Y. Wang, K. Yao and W. Lv, *Appl. Catal., B*, 2017, **207**, 103–113.
16 A. Aboueisha, *Toxicol. in Vitro*, 2006, **20**, 601–607.
17 F. Wang, Y. Wang, Y. Li, X. Cui, Q. Zhang, Z. Xie, H. Liu, Y. Feng, W. Lv and G. Liu, *Dalton Trans.*, 2018, **47**(20), 6924–6933.
18 Z. Wu, J. Fang, Y. Xiang, C. Shang, X. Li, F. Meng and X. Yang, *Water Res.*, 2016, **104**, 272.
19 R. Zhang, Y. Yang, C. H. Huang, N. Li, H. Liu, L. Zhao and P. Sun, *Environ. Sci. Technol.*, 2016, **50**, 2573.
20 S. Wang and J. Wang, *Chemosphere*, 2017, **191**, 97–105.
21 M. Q. Yang, B. Weng and Y. J. Xu, *Langmuir*, 2013, **29**, 10549–10558.
22 Y. Ding, L. Zhu, N. Wang and H. Tang, *Appl. Catal., B*, 2013, **129**, 153–162.
23 P. Laokul, V. Amornkitbamrung, S. Seraphin and S. Maensiri, *Curr. Appl. Phys.*, 2011, **11**, 101–108.
24 X. Zhang, M. Feng, R. Qu, H. Liu, L. Wang and Z. Wang, *Chem. Eng. J.*, 2016, **301**, 1–11.
25 C. Qi, X. Liu, C. Lin, H. Zhang, X. Li and J. Ma, *Chem. Eng. J.*, 2017, **315**, 201–209.
26 M. C. Dodd, M. O. Buffle and U. V. Gunten, *Environ. Sci. Technol.*, 2006, **40**, 1969–1977.
27 O. S. Furman, A. L. Teel and R. J. Watts, *Environ. Sci. Technol.*, 2010, **44**, 6423–6428.
28 I. M. Kolthoff and I. K. Miller, *J. Am. Chem. Soc.*, 1951, **73**, 1–30.
29 M. Pagano, A. Volpe, G. Mascolo, A. Lopez, V. Locaputo and R. Ciannarella, *Chemosphere*, 2012, **86**, 329–334.

30 G. S. Timmins, K. J. Liu, E. J. Bechara, Y. Kotake and H. M. Swartz, *Free Radical Biol. Med.*, 1999, **27**, 329.
31 P. Chen, F. Wang, Z. F. Chen, Q. Zhang, Y. Su, L. Shen, K. Yao, Y. Liu, Z. Cai and W. Lv, *Appl. Catal., B*, 2017, **204**, 250–259.
32 J. Kang, X. Duan, C. Wang, H. Sun, X. Tan, M. O. Tade and S. Wang, *Chem. Eng. J.*, 2018, **332**, 398–408.
33 Y. Ren, L. Lin, J. Ma, J. Yang, J. Feng and Z. Fan, *Appl. Catal., B*, 2015, **165**, 572–578.
34 T. N. Das, R. E. Huie and P. Neta, *J. Phys. Chem. A*, 1999, **103**, 3581–3588.
35 G. P. Anipsitakis and D. D. Dionysiou, *Environ. Sci. Technol.*, 2003, **37**, 4790.
36 X. Duan, C. Su, J. Miao, Y. Zhong, Z. Shao, S. Wang and H. Sun, *Appl. Catal., B*, 2018, **220**, 626–634.
37 X. Duan, H. Sun, Z. Shao and S. Wang, *Appl. Catal., B*, 2018, **224**, 973–982.
38 X. Duan, H. Sun and S. Wang, *Acc. Chem. Res.*, 2018, **51**, 678–687.
39 H. Lee, H. J. Lee, J. Jeong, J. Lee, N. B. Park and C. Lee, *Chem. Eng. J.*, 2015, **266**, 28–33.
40 R. Li, J. Kong, H. Liu, P. Chen, G. Liu, F. Li and W. Lv, *RSC Adv.*, 2017, **7**, 22802–22809.
41 J. Kuang, J. Huang, B. Wang, Q. Cao, S. Deng and G. Yu, *Water Res.*, 2013, **47**, 2863–2872.
42 R. Zhang, P. Sun, T. H. Boyer, L. Zhao and C. H. Huang, *Environ. Sci. Technol.*, 2015, **49**, 3056.
43 X. Liu, X. Zhang, K. Shao, C. Lin, C. Li, F. Ge and Y. Dong, *RSC Adv.*, 2016, **6**, 20938–20948.
44 L. Hu, A. M. Stemig, K. H. Wammer and T. J. Strathmann, *Environ. Sci. Technol.*, 2011, **45**, 3635–3642.
45 Y. Ji, W. Xie, Y. Fan, Y. Shi, D. Kong and J. Lu, *Chem. Eng. J.*, 2016, **286**, 16–24.